Kinematic and dynamic analogies between planar biped robots and the reaction mass pendulum (RMP) model

Ambarish Goswami

Honda Research Institute, Mountain View, CA 94041, U.S.A.

agoswami@honda-ri.com

***Abstract*—In order to simplify dynamic analysis, humanoid robots are often abstracted with various versions of the inverted pendulum model. However, most of these models do not explicitly characterize the robot's rotational inertia, a critical component of its dynamics, and especially of its balance. To remedy this, we have earlier introduced the *Reaction Mass Pendulum (RMP)*, an extension of the inverted pendulum, which models the rotational inertia and angular momentum of a robot through its centroidal composite rigid body (CCRB) inertia. However, we presented only the kinematic mapping between a robot and its corresponding RMP.**

Focussing in-depth on planar mechanisms, here we derive the dynamic equations of the RMP and explicitly compute the parameters that it must possess in order to establish equivalence with planar compass gait robot. In particular, we show that, a) an angular momentum equality between the robot and RMP does not necessarily guarantee kinetic energy equality, and b) a cyclic robot gait may not result in a cyclic RMP movement.

The work raises the broader question of how quantitatively similar the simpler models of humanoid robot must be in order for them to be of practical use.

I. Background and Motivation

Humanoid gait is often modeled with various versions of the inverted pendulum, such as the 2D and 3D linear inverted pendulums (LIP)[14], [13], the cart-table model[12], the variable impedance LIP[26], the spring-loaded inverted pendulum[2], and the angular momentum pendulum model (AMPM)[15], [16]. These reduced biped models have been very beneficial in the analysis and control of human and humanoid gait. The inverted pendulum models allow us to ignore the movements of the individual limbs of the humanoid and instead focus on two points of fundamental importance - the center of pressure (CoP) and the center of mass (CoM) - and the line joining them.

A limitation of the above models is that they represent the entire humanoid body only as a point mass and do not characterize the significant rotational inertia (except [15], [16]). The rotational inertia and the associated angular momentum are important components of humanoid movement and especially of balance, as have been reported [1], [9]). Direct manipulation of angular and linear momentum has been suggested as a reasonable, and sometimes preferable, way to control a robot [10], [11], [27].

Reaction Mass Pendulum: In order to explicitly model the rotational inertia and angular momentum of a humanoid we have earlier proposed the Reaction Mass Pendulum (RMP) model[18]. An RMP is essentially an inverted pendulum with its point mass replaced by an actuated extended-body mass that can rotate about the robot CoM. Fig. 1 shows the mechanical models of a 3D and a planar RMP. The RMP body mass captures the centroidal composite rigid body (CCRB) inertia of the robot, which is the instantaneous generalized inertia of the entire robot projected at its CoM. Additionally, for a particular rotational velocity of this extended mass, the centroidal angular momentum of the RMP equals to that of the robot.

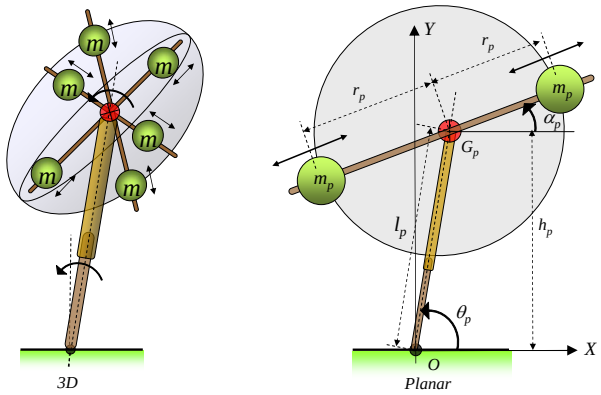

Fig. 1. Conceptual mechanical realization of the 3D and planar RMP. The RMP consists of a massless leg connecting the CoP and CoM, and a rotating body. In 3D, the rotating ellipsoidal body is mechanically equivalent to six equal masses on three mutually perpendicular rotating tracks. The body of a planar RMP reduces to a wheel and is equivalent to a pair of equal masses on a linear track. The CoM of the RMP is fixed at the common mid point of the track(s). This is the point about which the tracks themselves can rotate.

The movement of a humanoid robot results in a corresponding movement of the RMP. The change in robot's CCRB inertia is reflected in 3D by the changing shape, size and orientation of the ellipsoidal reaction mass, see Fig. 2. In plane, the radius of the rotational velocity of the inertia wheel will continuously change.

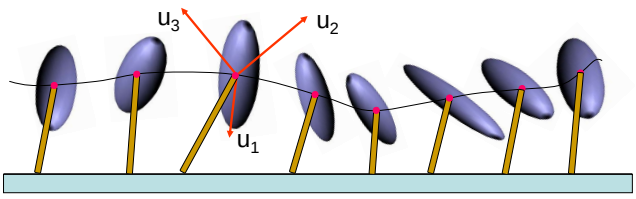

Fig. 2. As the humanoid moves, so does its RMP. Depending on the particular gait, the length of the RMP leg as well as the shape, size and orientation of the 3D reaction mass ellipsoid changes.

Focus of this paper: In our previous work we only presented the technique of kinematic mapping necessary to generate the RMP model starting from a robot at a given configuration. In this paper, we additionally derive the dynamic and energy parameters of a planar RMP and compare them with a planar robot. The decision to focus on planar robot models, and in particular the compass gait model, is to take advantages of analytical exploration. Many of the present findings are, nevertheless, valid for 3D models.

The comparison between humanoid robots and their RMP counterparts brings us to the broader topic of the extent of validity of reduced models in the dynamic analysis and control of humanoids. A humanoid controller based on a reduced model assumes that the humanoid has the same dynamics as that of the reduced model. The differences between the robot dynamics, which is substantially more complex than that of the reduced model, is treated as an error and compensated by the controller. If the robot behavior is reasonably captured by the reduced model, the discrepancy between their dynamics is not dramatic, and the compensation is generally successful.

What makes a dynamic model an acceptable reduced model of a more complex system? Are there criteria that the reduced model must satisfy for it to be practically admissible? To our knowledge, a comprehensive answer to this question has not emerged and each case is treated individually. While we do not seek to address this question in this paper, the process of a thorough comparison of two dynamic systems puts us in the right reference frame to pose such a question.

II. Compass gait biped

The biped robot model used in this paper is the so-called compass-gait model[8], see Fig. 3. The model has a double pendulum geometry and consists of two kneeless legs each having a point mass, and a third point mass is coincident with the hip joint. Despite its simplicity, this robot may exhibit autonomous "dynamic gait" [19] on a descending slope, even when the joints are unpowered. Researchers continue to actively study this model and suggest control laws of increasing complexity, depth and elegance[4], [3], [24].

The robot gait consists of successive stages of swing and ground impact. The robot can be powered through one motor at the hip and another at the ground contact point of the stance leg ("stance ankle"). After briefly reviewing the kinematics and dynamics of compass gait robot, which are known, we will introduce the expressions for the aggregate moment of inertia, the angular momentum and the momentum matrix of this model, all defined at the CoM.

A. Kinematics

The two legs of the robot are identical. The robot has three point masses, one at hip (m_H) and one on each leg (m). The leg masses are located at distances a and b, respectively, from the leg tip and the hip. The total mass of the robot is $M = 2m+m_h$ and the *mass ratio* is defined as $\mu = \frac{m_H}{m}$. Therefore, $M = (2+\mu)m = \mu' m$. The leg length is $l = a + b$ and the *length ratio* is defined as $\beta = \frac{a}{b}$, resulting in $l = (\beta+1)b = \beta' b$. We use the nominal values of $\mu = 2$ and $\beta = 1$. Note that the robot's geometry is completely determined by its interleg angle 2α, where $2\alpha = (\theta_1 - \theta_2)$. In this paper we will make frequent use of the parameters μ' and β'.

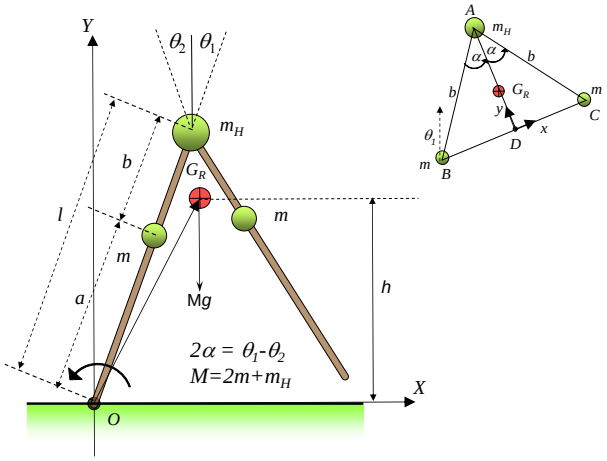

Fig. 3. Compass gait biped robot model. See Section II for description. The three masses are located at the vertices of an isosceles triangle (right, top).

B. Dynamics

The CoM coordinates (x_{G_R}, y_{G_R}) of the robot are given by,

$$x_{G_R} = \frac{b}{\mu'}[\rho \sin\theta_1 - \sin\theta_2] \tag{1}$$

$$y_{G_R} = \frac{b}{\mu'}[\rho \cos\theta_1 - \cos\theta_2] \tag{2}$$

where $\rho = (\mu'\beta' - 1)$ such that $(m_H l + ma + ml) = mb\rho$.

The governing equations of the robot consist of nonlinear differential equations for the swing stage and algebraic equations for the instantaneous ground impact. The swing stage equations can be derived using Lagrange's method starting from the potential and kinetic energies of the robot, PE_R and KE_R, respectively,

$$PE_R = bmg\,(\rho\cos\theta_1 - \cos\theta_2) \tag{3}$$

$$KE_R = 0.5m\,b^2[\zeta\,\dot\theta_1^2 - 2\beta'\cos 2\alpha\,\dot\theta_1\,\dot\theta_2 + \dot\theta_2^2] \tag{4}$$

where, $\zeta = (\mu'\,\beta'^2 - 2\beta - 1)$. The swing stage equations, which are similar to those of a frictionless double pendulum, can be written as[8]:

$$\boldsymbol{H}(\boldsymbol{q})\,\ddot{\boldsymbol{q}} + \boldsymbol{C}(\boldsymbol{q},\dot{\boldsymbol{q}})\,\dot{\boldsymbol{q}} + \boldsymbol{\tau}_g(\boldsymbol{q}) = \boldsymbol{\tau}, \tag{5}$$

where $\boldsymbol{q} = [\theta_1\ \theta_2]^T$, $\boldsymbol{H}(\boldsymbol{q})$ is the 2×2 inertia matrix, $\boldsymbol{C}(\boldsymbol{q},\dot{\boldsymbol{q}})$ is a 2×2 matrix with the centrifugal coefficients, and $\boldsymbol{\tau}_g(\boldsymbol{q})$ is a 2×1 vector of gravitational torques at the joints. $\boldsymbol{\tau}$ is a 2×1 vector of joint torques[1].

[1]The form of Eq. 5 is valid for both the robot and the RMP. We will use subscript $_R$ to denote the robot and $_P$ to denote the planar RMP. $\boldsymbol{H}_R$ and $\boldsymbol{H}_P$ thus means $\boldsymbol{H}(\boldsymbol{q})$ for the robot and the RMP, respectively.

C. Centroidal composite rigid body (CCRB) inertia

Instead of using general equations for deriving the CCRB inertia[2] of the compass gait robot[18], [21], we exploit the simplicity of the planar robot and adopt a more direct method. At any given configuration, the spatial arrangement of the three masses of the compass gait robot can be represented on an isosceles triangle ABC, as seen in Fig. 3. The global orientation of the triangle is given by θ_1, the support leg angle of the robot.

The CCRB inertia of the three point masses is $I_{G_R} = m(BG_R)^2 + m(CG_R)^2 + m_H(AG_R)^2$. We can show,

$$I_{G_R} = 2mb^2\left[1 - \frac{2\cos^2\alpha}{\mu'}\right] \tag{6}$$

where we have used the fact, $AG_R = AD - G_RD = \frac{2b}{\mu'}\cos\alpha$ and $CG_R = BG_R = b\sqrt{1 - \frac{4(1+\mu)}{\mu'^2}\cos^2\alpha}$.

For a planar robot the centroidal moment of inertia is a scalar. There is no inherent way to visualize it, unlike in case of 3D robots, which has three perpendicular axes naturally given by the eigenvectors of the centroidal inertia ellipsoid[18]. The maximum value of I_{G_R} is $2mb^2$ which occurs when $\alpha = 90°$.

D. Centroidal momentun and centroidal momentum matrix

The linear momentum $\boldsymbol{l}_R$ of the robot is computed by multiplying the CoM velocity with the aggregate mass,

$$\boldsymbol{l}_R = \mu' m(\dot{x}_{G_R}\,\hat{\boldsymbol{i}} + \dot{y}_{G_R}\,\hat{\boldsymbol{j}}) \tag{7}$$

The centroidal angular momentum k_{G_R} – the robot's angular momentum referenced to its CoM – is the sum of angular momenta of its individual mass elements, after projecting each to the robot's CoM[18].

$$k_{G_R} = mb^2\left[1 - \frac{2\cos^2\alpha}{\mu'}\right](\dot{\theta}_1 + \dot{\theta}_2), \tag{8}$$

$\boldsymbol{A}_{G_R}(\boldsymbol{q})$, the centroidal momentum matrix (CMM) of the robot maps its joint velocities to its centroidal angular momentum[21] according to

$$\boldsymbol{h}_{G_R} = \boldsymbol{A}_{G_R}(\boldsymbol{q})\,\dot{\boldsymbol{q}}, \tag{9}$$

where $\boldsymbol{h}_{G_R} = [k_{G_R} \quad l_{R_x} \quad l_{R_y}]^T$ is the centroidal *spatial* momentum vector. We can write,

$$\boldsymbol{A}_{G_R} = mb\begin{bmatrix} b(1 - \frac{2\cos^2\alpha}{\mu'}) & b(1 - \frac{2\cos^2\alpha}{\mu'}) \\ \rho\cos\theta_1 & -\cos\theta_2 \\ -\rho\sin\theta_1 & \sin\theta_2 \end{bmatrix}. \tag{10}$$

The CMM matrix is recognized as an important matrix in angular momentum control of humanoids[11], [7] and its structure and properties are being studied[21].

Next we will study the dynamic equations and other physical quantities of importance of the planar RMP.

[2]The composite rigid body (CRB) inertia was introduced in robotics to obtain efficient computational algorithms for robot dynamics[28]. In physics and geometric dynamics the concept is called the locked inertia.

III. Planar reaction mass pendulum (RMP) model

The planar RMP is dynamically analogous to the reaction wheel pendulum [5], [20], [25], except that the RMP has a variable CCRB whereas the wheel's inertia is constant[3]. At any given configuration of the RMM, its CCRB inertia can be represented by the pair of point masses m_p. The generalized coordinates and generalized forces of the planar RMP are $\boldsymbol{q}_P = (\theta, \alpha, r_l, r_P)$ and $\boldsymbol{\tau}_P = (\tau_\theta, f_l, \tau_\alpha, f_r)$, respectively (refer to Fig. 1). When $r_P = 0$, the planar RMP reduces to a traditional inverted pendulum. If, in addition, we constrain the CoM to stay at a constant horizontal level, we obtain the planar LIP.

A. Dynamic Equations

The motion equations of the planar RMP can be obtained starting from its potential and kinetic energies, PE_P and KE_P.[4] These are given by

$$PE_P = 2m_P\,g\,h_P = 2m_P\,g\,l_P\,\sin\theta_P \tag{11}$$

$$KE_P = m_P(\dot{l}_P^2 + \dot{r}_P^2 + l_P^2\dot{\theta}_P^2 + r_P^2\dot{\alpha}_P^2) \tag{12}$$

We can derive the dynamic equations as follows:

$$\frac{1}{2m_P}\begin{bmatrix}\tau_{\theta_P}\\ f_l\\ \tau_{\alpha_P}\\ f_r\end{bmatrix} = \begin{bmatrix} l_P^2 & 0 & 0 & 0\\ 0 & 1 & 0 & 0\\ 0 & 0 & r_P^2 & 0\\ 0 & 0 & 0 & 1\end{bmatrix}\begin{bmatrix}\ddot{\theta}_P\\ \ddot{l}_P\\ \ddot{\alpha}_P\\ \ddot{r}_P\end{bmatrix}$$
$$+\begin{bmatrix} l_P\dot{l}_P & l_P\dot{\theta}_P & 0 & 0\\ -l_P\dot{\theta}_P & 0 & 0 & 0\\ 0 & 0 & r_P\dot{r}_P & r_P\dot{\alpha}_P\\ 0 & 0 & -r_P\dot{\alpha}_P & 0\end{bmatrix}\begin{bmatrix}\dot{\theta}_P\\ \dot{l}_P\\ \dot{\alpha}_P\\ \dot{r}_P\end{bmatrix} + g\begin{bmatrix} l_P\cos\theta_P\\ \sin\theta_P\\ 0\\ 0\end{bmatrix} \tag{13}$$

B. Linear and angular momenta

The CoM location of the RMP is given by,

$$x_{G_P} = l_P\,\cos\theta_P, \qquad y_{G_P} = l_P\,\sin\theta_P \tag{14}$$

whereas its linear momentum is expressed as,

$$\boldsymbol{l}_P = 2m_P[(\dot{l}_P\cos\theta_P - l_P\dot{\theta}_P\sin\theta_P)\hat{\boldsymbol{i}} + (\dot{l}_P\sin\theta_P + l_P\dot{\theta}_P\cos\theta_P)\hat{\boldsymbol{j}}] \tag{15}$$

The CCRB inertia of the RMP has the compact form,

$$I_{G_P} = 2\,m_P\,r_P^2 \tag{16}$$

from which the centroidal angular momentum and its derivative[5] can be computed as,

$$k_{G_P} = I_{G_P}\,\dot{\alpha}_P = 2m_P\,r_P^2\,\dot{\alpha}_P \tag{17}$$

$$\dot{k}_{G_P} = 2m_P r_P(r_P\ddot{\alpha}_P + 2\dot{r}_P\dot{\alpha}_P). \tag{18}$$

[3]Reaction wheel pendulum consists of an actuated spinning wheel pin-jointed to a rigid rod. A spinning reaction wheel or an inertia wheel has been suggested as a means of stabilizing the lateral biped dynamics[17], [23].

[4]Note that KE_P does not contain any coupled terms of the form $\dot{\theta}_P\dot{\alpha}_P$ and $\dot{l}_P\dot{\theta}_P$. Neither does it depend on θ_P and α_P, rendering them cyclic variables([29], pp. 426).

[5]Angular momentum rate change referred to at the CoP $\dot{k}_O = \boldsymbol{OG}_P \times M\boldsymbol{g}$ from which follows $\dot{k}_O = \dot{k}_{G_P} + \boldsymbol{OG}_P \times M\ddot{\boldsymbol{OG}}_P$.

Note that $\dot{k}_{G_P}$ is also expressed as, $\dot{k}_{G_P} = \boldsymbol{G}_P\boldsymbol{O} \times \boldsymbol{R}$, in which the ground reaction force, $\boldsymbol{R}$, is computed from,

$$\boldsymbol{R} = M(\ddot{\boldsymbol{O}}\boldsymbol{G}_P - g). \tag{19}$$

Similar to Eq. 10 the CMM of the planar RMP defining the mapping relationship $\boldsymbol{h}_{G_P} = \boldsymbol{A}_{G_P}(\boldsymbol{q}_P)\,\dot{\boldsymbol{q}}_P$ is given by,

$$\boldsymbol{A}_{G_P} = m_p \begin{bmatrix} 0 & 0 & 2r_p^2 & 0 \\ -l_P \sin\theta_P & \cos\theta_P & 0 & 0 \\ -l_P \cos\theta_P & \sin\theta_P & 0 & 0 \end{bmatrix}. \tag{20}$$

IV. Establishing equivalence between compass gait robot and planar RMP

The similarities and differences between a compass gait robot and a planar RMP are presented in Table. I. In a sense, the robot and the RMP are two vastly different systems given by their different sets of generalized coordinates and forces. Yet, by construction, the total mass, CoM position, centroidal moment of inertia and potential energy of the RMP are identical to those of the robot.

TABLE I
Comparison between Compass Gait Biped and planar RMP

Variables and quantities	Compass Gait Robot	Planar RMP
Generalized coordinates	$\boldsymbol{q}_R = [\theta_1, \theta_2]^T$	$\boldsymbol{q}_P = [\theta_P, l_P, \alpha_P, r_P]^T$
Generalized forces	$\boldsymbol{\tau}_R = [u_1, u_2]^T$	$\boldsymbol{\tau}_P = [\tau_\theta, f_l, \tau_\alpha, f_r]^T$
Geometry	a, b, $(b = \beta a)$ $a + b = l$	None fixed
CoM position	Function of $\boldsymbol{q}_R$, see Eqs. 1 and 2	$x = l_P \cos\theta_P$, $y = l_P \sin\theta_P$
Mass	m, m_H, $(m_H = \mu m)$	$m_P = \frac{M}{2}$, $(M = 2m + m_H)$
Centroidal moment of inertia (CCRBI)	$I_{G_R} = 2mb^2[1 - \frac{2}{2+\mu}\cos^2\alpha]$	$I_{G_P} = 2m_P r_P^2$ so, $r_P = \sqrt{\frac{I_{G_P}}{2m_P}}$
Potential Energy	$PE_R = Mgh$,	$PE_P = 2m_P\, g\, h_P$, $(h_P = h)$
Kinetic Energy	KE_R : Eq. 4	KE_P : Eq. 12
Linear momentum	$\boldsymbol{l}_R$: Eq. 7	$\boldsymbol{l}_P$: Eq. 15
Angular momentum	k_{G_R} : Eq. 8	k_{G_P} : Eq. 17

A. Computation of θ_P, l_P and r_P

In this section we determine the quantities θ_P, l_P and r_P, these quantities depend on the joint angles, and not velocities of the compass gait robot.

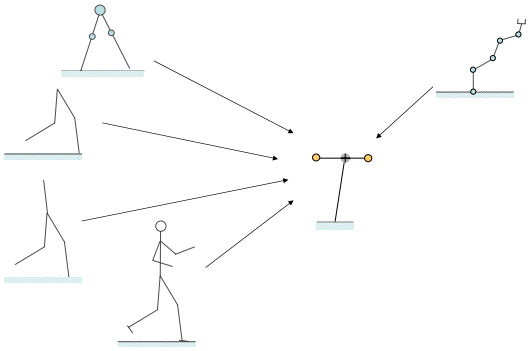

Fig. 4. Schematic diagram showing that planar robots of completely general kinematics, both humanoid and fixed-based manipulators, can be represented by the same planar RMP model.

1) Generalized coordinates and forces: The robot has two generalized variables (coordinates and forces) whereas the RMP has four. This might appear surprising and counter-productive to the underlying theme of model reduction. However, note that the planar RMP model can represent not just the compass gait robot considered here, but the entire range of planar humanoid robots, as well as planar manipulators no matter how complex, as schematically shown in Fig. 4.

2) Geometry: While the robot has fixed geometry, the geometry of RMP is continuously changing. In fact, the two length parameters, l_P and r_P of the RMP, are generalized coordinates.

3) CoM location: The CoM of the robot and the RMP are required to coincide, which specifies the values of l_p and θ_p as

$$l_p = \sqrt{x_{G_R}^2 + y_{G_R}^2} = \frac{b}{\mu'}\sqrt{\rho^2 + 1 - 2\rho\cos 2\alpha_R} \tag{21}$$

$$\theta_p = \arctan 2\left(\frac{y_{G_R}}{x_{G_R}}\right) = \arctan 2\left[\frac{\rho\cos\theta_1 - \cos\theta_2}{\rho\sin\theta_1 - \sin\theta_2}\right] \tag{22}$$

4) Mass and inertia: The total mass of the robot and the RMP are to be equal, from which we compute m_P as,

$$m_P = \mu'/2 \tag{23}$$

5) Centroidal composite rigid body inertia: CCRB inertia continuously changes for both the robot and the RMP. For the RMP, the CCRB inertia depends only on r_P. In fact, r_P can be computed using the requirement $I_{G_R} = I_{G_P}$ as,

$$r_p = \frac{b\sqrt{2}}{\mu'}\sqrt{\mu' - 2\cos^2\alpha} \tag{24}$$

As an illustration, Fig. 5 shows the equivalence between a compass gait robot and the planar RMP.

6) Potential and kinetic energies: Potential energy depends only on the total mass and the CoM height. Since the CoM location is identical for both the robot and the RMP, it automatically follows that $PE_R = PE_P$. For kinetic energy, unfortunately, there is no such guarantee. KE_R and KE_P may be unequal.

Out of the four generalized coordinates of the planar RMP, we have so far determined only three. The fourth, α_P, is

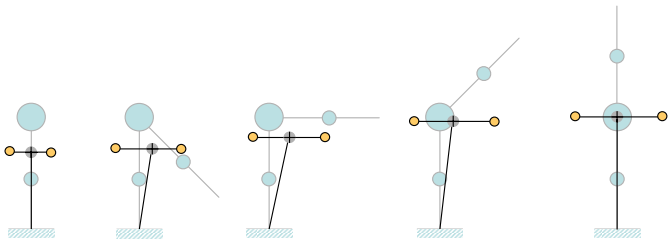

Fig. 5. Kinematic equivalence between compass gait robot and planar RMP. Compass gait robot is shown with light blue mass and grey links in the background, its inter-leg angle increasing from 0° to 180°. Superimposed on each robot configuration is the corresponding RMP. The leg of the RMP extends from the robot's CoP to CoM.

indirectly obtained from angular momentum equality between the robot and the RMP, as we see next.

B. Angular momentum equivalence and computation of α_P

To compute the RMP body orientation α_P, one has to first compute $\dot{\alpha}_P$ through angular momentum equivalence between robot and RMP, and then integrate it. For compass gait robot, $\dot{\alpha}_P$ can be obtained from Eq.17, while setting $k_{G_P} = k_{G_R}$,

$$\dot{\alpha}_P = I_{G_P}^{-1}\, k_{G_R} = \frac{1}{2m_P r_P^2}\, k_{G_R} \tag{25}$$

Next, the expressions for r_p and k_{G_R} can be plugged in using Eq. 24 and Eq. 8, respectively. From Eq. 25 we obtain,

$$\dot{\alpha}_P = \frac{\dot{\theta}_1 + \dot{\theta}_2}{2} \tag{26}$$

which can be integrated to obtain $\alpha_P = \frac{\theta_1+\theta_2}{2}$. To begin integration, we can arbitrarily set $\alpha_P(0) = 0$.

In analogy to the RMP, what does $\dot{\alpha}_P$ signify for the compass gait robot? $\dot{\alpha}_P$ together with k_{G_R} is nothing but the rotational counterpart of the linear momentum l_R and the CoM translational velocity. The same way as the CoM velocity depicts an average translational velocity of a robot, $\dot{\alpha}_P$ is seen as its fictitious centroidal angular velocity or the whole-body angular velocity[22]. Furthermore, α_P is seen as the whole-body angular excursion[22] although it cannot be a-priori linked to the geometry or dynamics of the robot. An alternative description of average angular velocity, derived from kinetic energy equivalence, is presented in [6].

The physical interpretation of the centroidal angular velocity of a robot is therefore the following: At any instant, if the robot is replaced by its equivalent CCRB inertia, the angular velocity with which this inertia must rotate in order to possess the prescribed angular momentum is the centroidal angular velocity.

C. Torque mapping between planar RMP and planar biped

We have derived a mapping of generalized coordinates between the compass gait robot and the planar RMP. A complete mapping of state variables can be established by obtaining the time derivatives (analytic, in the current case) of the generalized coordinates.

The mapping of generalized forces is more involved. One must first determine the purpose of such a mapping. As an example, we explore the case of torque mapping where the objective is to maintain the equivalence of rate of change of centroidal angular momentum between the RMP and the robot.

Taking time derivative of Eq. 9 we obtain, for both robot and RMP,

$$\dot{\boldsymbol{h}}_G = \boldsymbol{A}_G\, \ddot{\boldsymbol{q}} + \dot{\boldsymbol{A}}_G\, \dot{\boldsymbol{q}} \tag{27}$$

from which we extract $\ddot{\boldsymbol{q}}$

$$\ddot{\boldsymbol{q}} = \boldsymbol{A}_G^{+}\,(\,\dot{\boldsymbol{h}}_G - \dot{\boldsymbol{A}}_G\, \dot{\boldsymbol{q}}). \tag{28}$$

Plugging $\ddot{\boldsymbol{q}}$ in the dynamic equations Eq. 5 we obtain,

$$\dot{\boldsymbol{h}}_G = \boldsymbol{A}_G \boldsymbol{H}^{-1}(\boldsymbol{\tau} - \boldsymbol{C}\dot{\boldsymbol{q}} - \boldsymbol{\tau}_g) + \dot{\boldsymbol{A}}_G\dot{\boldsymbol{q}} \tag{29}$$

which is of the form

$$\dot{\boldsymbol{h}}_G = \boldsymbol{\mathcal{W}}\boldsymbol{\tau} + \boldsymbol{\mathcal{X}} \tag{30}$$

where $\boldsymbol{\mathcal{W}} = \boldsymbol{A}_G\boldsymbol{H}^{-1}$ and $\boldsymbol{\mathcal{X}} = (\dot{\boldsymbol{A}}_G - \boldsymbol{\mathcal{W}}\boldsymbol{C})\dot{\boldsymbol{q}} - \boldsymbol{\mathcal{W}}\boldsymbol{\tau}_g$. The position and velocity dependent terms are contained in $\boldsymbol{\mathcal{X}}$. Eq. 30 is an affine relationship between joint torques and the rate of change of centoridal spatial momentum. Setting $\dot{\boldsymbol{h}}_{G_R} = \dot{\boldsymbol{h}}_{G_P}$, we readily obtain,

$$\boldsymbol{\mathcal{W}}_R\boldsymbol{\tau}_R + \boldsymbol{\mathcal{X}}_R = \boldsymbol{\mathcal{W}}_P\boldsymbol{\tau}_P + \boldsymbol{\mathcal{X}}_P \tag{31}$$

which yields an expression for $\boldsymbol{\tau}_P \rightarrow \boldsymbol{\tau}_R$ mapping

$$\boldsymbol{\tau}_R = \boldsymbol{\mathcal{W}}_R^{+}\,[\boldsymbol{\mathcal{W}}_P\boldsymbol{\tau}_P + (\boldsymbol{\mathcal{X}}_P - \boldsymbol{\mathcal{X}}_R)] \tag{32}$$

Note that $\boldsymbol{\mathcal{W}}_R$ is a rectangular matrix and the issues regarding its appropriate inverse need to be resolved.

For the planar RMP, Eq. 29 can be shown to result $\dot{k}_{G_P} = \tau_\alpha$. It is precisely because the centroidal angular momentum rate change is explicitly captured by a single joint torque, that we have chosen the RMP model.

V. Simulation and Discussion

To support our analytical findings we have used simulation data of a compass gait biped[6]. The data contain the kinematic variables during a few stable walk cycles of a compass gait biped robot on an inclined slope. Using the techniques described in this paper we have mapped the biped robot data to the equivalent planar RMP variables. Fig. 6, Fig. 7, and Fig. 8 show the time evolution plots of the generalized coordinates, generalized forces and the CCRB inertia of the RMP, respectively. The generalized forces were computed using Eq.13 through intermediate steps computation steps of generalized accelerations.

Fig. 9 shows the plots of kinetic energies of the robot and the RMP. Although there were no KE-specific restriction placed on the RMP model variables, the kinetic energies of the models tend to be in the neighborhood of each other.

Fig. 10 presents the plots of both α_P and $\dot{\alpha}_P$. The remarkable finding in this plot is that although $\dot{\alpha}_P$ is a cyclic quantity,

[6]The data was given by Dr. Fumihiko Asano. The bipedal gait was generated in accordance with the method of virtual passive dynamic walking[4].

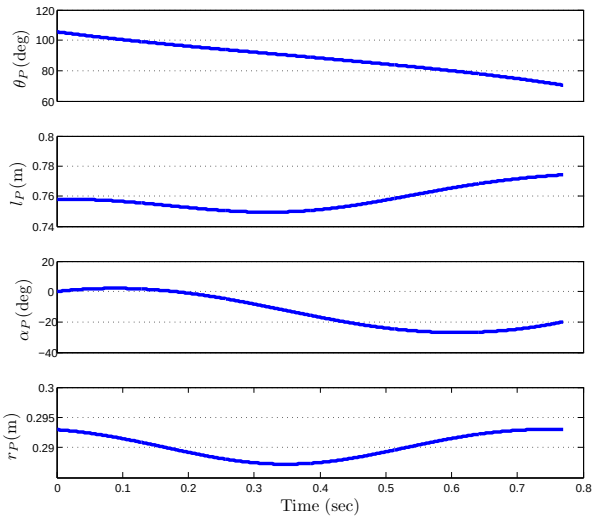

Fig. 6. The generalized coordinates of the RMP from one gait cycle.

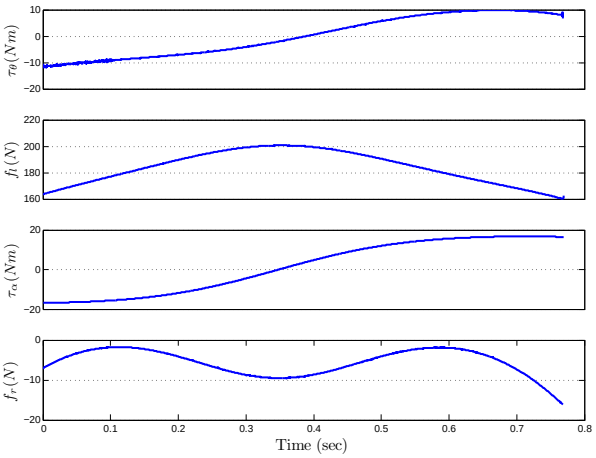

Fig. 7. The generalized forces of the RMP from one gait cycle.

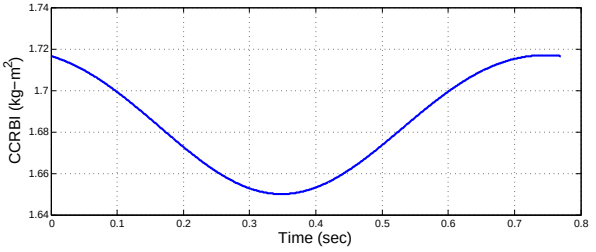

Fig. 8. CCRBI plot of both robot and planar RMP.

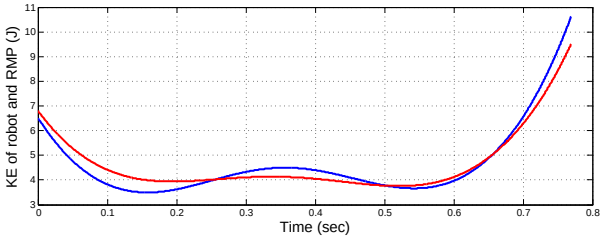

Fig. 9. Kinetic energy plot of robot (in red) and planar RMP (in blue).

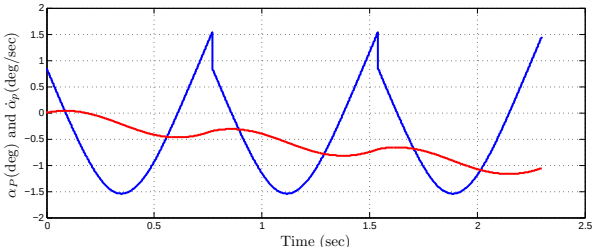

Fig. 10. Rotational angle α_P (in red) and angular velocity $\dot{\alpha}_P$ (in blue) of RMP.

α_P is not. Applied to the RMP, this implies that the pendulum body does not repeat its trajectory at each gait cycle. In fact, as the plot shows, the body rotation fluctuates but steadily rotates backwards as time goes on. The significance of this finding vis-a-vis the centroidal angular velocity of the robot is not clear.

Finally, Fig. 11 shows the evolution of the centroidal angular momentum of the robot superposed on its 3D CoM trajectory. The positive to negative reversals of the angular momentum is a curious factor that deserves further study.

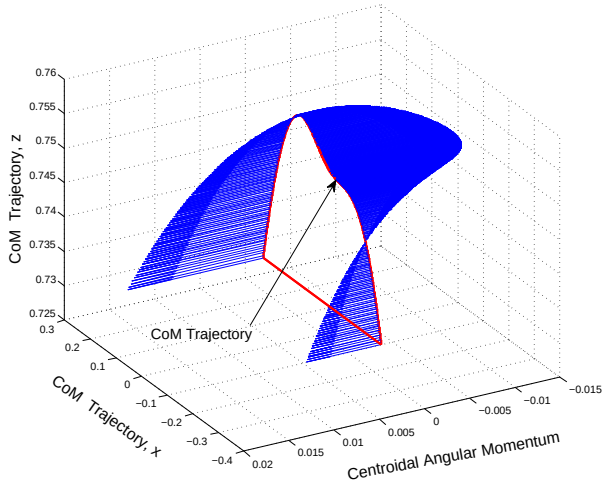

Fig. 11. Centroidal angular momentum of robot and RMP superposed on CoM trajectory. The magnitude of angular momentum is given by the length of the line projected outwards from the CoM trajectory.

VI. Conclusions and Future Work

We have explored the kinematic, dynamic and energy equivalence between planar biped robots and planar reaction mass pendulum (RMP) model. The RPM model is similar to the existing inverted pendulum humanoid models, but has an additional rotational mass to explicitly identify the centroidal rigid body inertia of the robot and, by extension, its centroidal angular momentum.

The RMP is an instantaneous capture of the aggregate kinematics and dynamics of a humanoid robot. We have derived the analytical dynamic equations of the planar RMP. By imposing equivalence between the robot and the RMP, we have expressed the mass and geometry parameters and the generalized coordinates of the RMP as functions of those of the

robot. Interestingly, one of the generalized coordinates can be ascertained through integration, only after the corresponding generalized velocity is determined. Through forward dynamics we can also compute the joint torques necessary for the RMP to mimic the corresponding motion of the planar robot.

We have shown that, a) an angular momentum equality between the robot and RMP does not necessarily guarantee kinetic energy equality, and b) a cyclic robot gait may not result in a cyclic RMP movement. A non-cyclic gait has ramifications for the humanoid gait planning and this issue needs to be further explored.

Regardless of the complexity of a planar robot, the RMP has a fixed 4-dimensional equivalent RMP. Having this standard model makes it easier to uniformly compare the dynamics of different humanoids. This is a task for the future. Also it will be interesting to consider the RMP equivalent of a fixed-base manipulator robot.

We are also exploring appropriate torque mappings between the compass gait robot and the RMP, as well the kinetic energy equivalence between the two models. Final objective of our work remains the formulation of control law for humanoid robots to which the current paper is another step.

ACKNOWLEDGMENT

I am grateful to Dr. Fumihiko Asano of RIKEN, Nagoya, Japan, for discussions on compass gait dynamics, and especially for providing me with his simulation data, which I used in Section. V. Fruitful discussions with David Orin and Jerry Pratt are acknowledged.

REFERENCES

[1] M. Abdallah and A. Goswami. A biomechanically motivated two-phase strategy for biped robot upright balance control. In *IEEE International Conference on Robotics and Automation (ICRA)*, pages 3707–3713, April 2005, Barcelona, Spain.

[2] R. Altendorfer, Uluc Saranli, H. Komsuoglu, D.E. Koditschek, H. Benjamin Brown, Martin Buehler, N. Moore, D. McMordie, and R. Full. Evidence for spring loaded inverted pendulum running in a hexapod robot. In D. Rus and S. Singh, editors, *Experimental Robotics VII*, pages 291 – 302. Springer-Verlag, 2001.

[3] F. Asano and Z.-W. Luo. On energy-efficient and high-speed dynamic biped locomotion with semicircular feet. In *IEEE/RSJ International Conference on Intelligent Robots and Systems (IROS)*, pages 5901–5906, October, Beijing, China 2006.

[4] F. Asano, Z.-W. Luo, and M. Yamakita. Biped gait generation and control based on a unified property of passive dynamic walking. 21(4):754–762, 2005.

[5] K. Astrom, A. Block, and M. Spong. *The Reaction Wheel Pendulum*. Downloadable from: http://decision.csl.uiuc.edu/ spong/main.htm, 2001.

[6] H. Essén. Average angular velocity. *European Journal of Physics*, 14:201–205, 1993.

[7] A. C. Fang and N. Pollard. Efficient synthesis of physically valid human motion. 22(3):417–426, 2003.

[8] A. Goswami, B. Thuilot, and B. Espiau. Compass-like biped robot part i: Stability and bifurcation of passive gaits. Technical report, INRIA, No. 2996, Oct. 1996.

[9] H. Herr and M. Popovic. Angular momentum in human walking. *The Journal of Experimental Biology*, 211:467–481, 2008.

[10] A. Hofmann. *Robust execution of biped walking tasks from biomechanical principles*. PhD thesis, MIT, AI Lab, 2006.

[11] S. Kajita, F. Kanehiro, K. Kaneko, K. Fujiwara, K. Harada, K. Yokoi, and H. Hirukawa. Resolved momentum control: humanoid motion planning based on the linear and angular momentum. In *IEEE/RSJ International Conference on Intelligent Robots and Systems (IROS)*, volume 2, pages 1644–1650, 2003, Las Vegas, NV, USA.

[12] S. Kajita, F. Kanehiro, K. Kaneko, K. Fujiwara, K. Harada, K. Yokoi, and H. Hirukawa. Biped walking pattern generation by using preview control of zero-moment point. In *IEEE International Conference on Robotics and Automation (ICRA)*, pages 1620–1626, 2003, Taipei, Taiwan.

[13] S. Kajita, F. Kanehiro, K. Kaneko, K. Yokoi, and H. Hirukawa. The 3d linear inverted pendulum mode: A simple modeling for a biped walking pattern generator. In *IEEE/RSJ International Conference on Intelligent Robots and Systems (IROS)*, pages 239–246, 2001, Maui, Hawaii.

[14] S. Kajita and K. Tani. Study of dynamic biped locomotion on rugged terrain. In *IEEE International Conference on Robotics and Automation (ICRA)*, pages 1405–1411, 1991.

[15] T. Komura, H. Leung, S. Kudoh, and J. Kuffner. A feedback controller for biped humanoids that can counteract large perturbations during gait. In *IEEE International Conference on Robotics and Automation (ICRA)*, pages 2001–2007, 2005, Barcelona, Spain.

[16] T. Komura, A. Nagano, H. Leung, and Y. Shinagawa. Simulating pathological gait using the enhanced linear inverted pendulum model. *IEEE Transactions on Biomedical Engineering*, 52(9):1502–1513, 2005, September.

[17] A. Kuo. Stabilization of lateral motionin passive dynamic walking. *International Journal of Robotics Research*, 18(9):917–930, 1999, September.

[18] S-H. Lee and A. Goswami. Reaction mass pendulum (RMP): An explicit model for centroidal angular momentum of humanoid robots. In *IEEE International Conference on Robotics and Automation (ICRA)*, pages 4667–4672, April 2007.

[19] T. McGeer. Passive dynamic walking. *International Journal of Robotics Research*, 9(2):62–82, 1990.

[20] R. Olfati-Saber. Stabilization of a flat underactuated system: the inertia wheel pendulum. In *40th Conference on Decision and Control*, pages 306–308, December 4-7 2001, Orlando, FL.

[21] D. Orin and A. Goswami. Centroidal momentum matrix of a humanoid robot: Structure and properties. In *IEEE/RSJ International Conference on Intelligent Robots and Systems (IROS)*, 2008, Nice, France.

[22] M. Popovic, A. Goswami, and H. Herr. Ground reference points in legged locomotion: Definitions, biological trajectories and control implications. *International Journal of Robotics Research*, 24(12):1013–1032, 2005.

[23] J Pratt. *Exploiting inherent robustness and and natural dynamics in the control of bipedal walking robots*. PhD thesis, MIT, 2000.

[24] M. W. Spong and F. Bullo. Controlled symmetries and passive walking. *IEEE Transactions on Automatic Control*, 50(7):1025–1031, July 2005.

[25] M. W. Spong, P. Corke, and R. Lozano. Nonlinear control of inertia wheel pendulum. *Automatica*, 37:1845–1851, February 2001.

[26] T. Sugihara and Y. Nakamura. Variable impedant inverted pendulum model control for a seamless contact phase transition on humanoid robot. In *IEEE International Conference on Humanoid Robots (Humanoids2003)*, pages 0–0, Oct 2003, Germany.

[27] J. Vermeulen, B. Verrelst, B. Vanderborght, D. Lefeber, and P. Guillaume. Trajectory planning for the walking biped.

[28] M. W. Walker and D. Orin. Efficient dynamic computer simulation of robotic mechanisms. *ASME Journal of Dynamic Systems, Measurement, and Control*, 104:205–211, Sept. 1982.

[29] E. Westervelt, J. W. Grizzle, C. Chevallereau, J. O. Choi, and B. Morris. *Feedback Control of Dynamic Bipedal Robot Locomotion*. CRC Press, Boca Raton, FL, 2007.